A Novel Approach to Unambiguous Doppler Beam sharpening for Forward-looking MIMO Radar

Yuan, Sen; Aubry, Pascal; Fioranelli, Francesco; Yarovoy, Alexander

DOI
10.1109/JSEN.2022.3215862

Publication date
2022

Document Version
Final published version

Published in
IEEE Sensors Journal

A Novel Approach to Unambiguous Doppler Beam Sharpening for Forward-Looking MIMO Radar

Sen Yuan, *Graduate Student Member, IEEE*, Pascal Aubry, Francesco Fioranelli, *Senior Member, IEEE*, and Alexander G. Yarovoy, *Fellow, IEEE*

***Abstract*—The ambiguity problem of targets in Doppler beam sharpening (DBS) with forward-looking radar is considered. While DBS is proposed earlier to improve the angular resolution of the radar while keeping the antenna aperture size limited, such a solution suffers from ambiguities in the case of targets positioned symmetrically with respect to the platform movement. To address this problem, an approach named unambiguous Doppler-based forward-looking multiple-input multiple-output (MIMO) radar beam sharpening scan (UDFMBSC) is proposed, based on the combination of MIMO processing and DBS. The performance of the proposed method is compared to existing approaches using simulated data with point-like and extended targets. The method is successfully verified using experimental data.**

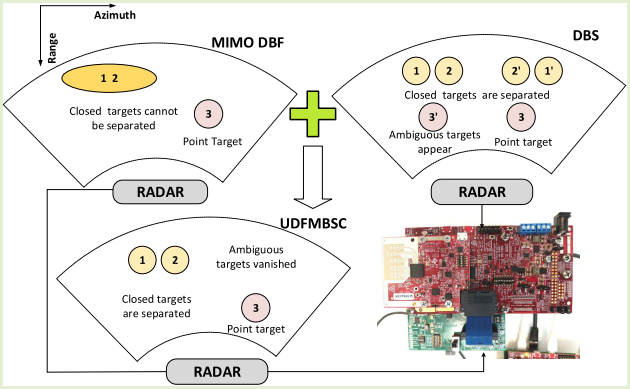

***Index Terms*—Beam scan, Doppler beam sharpening (DBS), forward-looking radar, multiple-input multiple-output (MIMO) radar processing.**

I. Introduction

THE success of autonomous vehicles strongly depends on their environment-sensing capabilities. Autonomous vehicles are equipped with multiple sensors, including radars, cameras, and lidars [1]. Among them, radar can provide accurate and direct measurements of the range, relative velocity, and angle of multiple targets; offer a long-range coverage of more than 200 m even in challenging weather or lighting conditions [2]; and be easily packaged behind the optically nontransparent fascia of the vehicle. Therefore, radar is typically used in current ADASs' tasks, such as adaptive cruise control (ACC) [3], forward collision avoidance (FCA) [4], lane-change assistance [5], or evasion assistance [6], and is considered one of the key technologies for next-generation autonomous vehicles [7].

Manuscript received 16 September 2022; accepted 15 October 2022. Date of publication 25 October 2022; date of current version 30 November 2022. The associate editor coordinating the review of this article and approving it for publication was Dr. Masood Ur Rehman. *(Corresponding author: Sen Yuan.)*

The authors are with the Microwave Sensing, Signals and Systems Group, Delft University of Technology, 2628CD Delft, The Netherlands (e-mail: s.yuan-3@tudelft.nl; p.j.aubry@tudelft.nl; f.fioranelli@tudelft.nl; a.yarovoy@tudelft.nl).

Digital Object Identifier 10.1109/JSEN.2022.3215862

Thanks to highly integrated and inexpensive mm-wave circuits, radar sensors operating in 77 GHz bands of the electromagnetic (EM) spectrum, known as mm-wave frequencies, have become popular [8]. Mm-wave radar can offer a large operational bandwidth providing sufficient range resolution. Doppler resolution is a function of chirp duration and the number of chirps used for the estimation, so it is limited by the coherent observation time, with better velocity resolution achieved by operating at high frequencies [9]. However, a weakness of current radar sensors is their poor angular resolution, meaning that two adjacent targets at the same distance but different azimuth or elevation angles may not be separated. For this reason, lidars are widely used in autonomous vehicles, thanks to their very fine angular resolution despite their cost.

The angular resolution of a radar depends on the antenna aperture. It, thus, is determined by the number and geometry of the transmit and receive channels, which are limited by the radar cost and packaging size. Large-aperture antenna arrays can be implemented via phased array [10] and multiple-input multiple-output (MIMO) array techniques [11] to achieve an improved angle resolution. Phased arrays typically use numerous antennas to form a large aperture to achieve a narrow beam width. However, they are usually not a feasible

option for automotive radar. MIMO radar technology exploits the spatial diversity of transmit and receive antenna arrays, thus providing an improved angle resolution with a limited number of antennas. Many direction of arrival (DOA) methods have been developed to gain resolution in the angular domain via signal processing, including minimum variance distortionless response (MVDR) [12], subspace-based methods such as multiple signal classification (MUSIC) [13], [14], and estimation of signal parameters via rational invariance techniques (ESPRITs) [15], sparse sensing-based approaches [16], the iterative adaptive approach (IAA) [17], [18], and harmonic analysis [19], [20]. However, the obtained angular resolution is still insufficient, limited by the physical azimuth beam width and the computational complexity of some of these methods.

Doppler beam sharpening (DBS) is an alternative way to achieve fine angular resolution for targets close to each other in automotive radar [21]. Synthetic aperture radar (SAR) [22] was actually first named as DBS when designed [23]. It utilizes the variations in the relative Doppler frequency shift of scatterers at different look angles with respect to the trajectory of radar. In this way, it forms a large effective (i.e., virtual) aperture array by moving a small antenna or array. This reduces the number of physical antennas required for imaging, thus providing a cost-effective solution for high-resolution imaging applications. Several researchers have investigated the use of DBS for imaging. Daniel et al. [21] investigated the application of DBS for the angular resolution refinement of low-Terahertz radar sensing. Mao et al. [24] combined DBS with the fast IAA to achieve high azimuth resolution in the forward-squint region. It is challenging to use this approach in the forward-looking direction, which is, especially, of interest for autonomous vehicles, because of two challenging problems. First, this approach has no or poor angular resolution for look angles equal or close to zero degrees, that is, $[-\epsilon, \epsilon]$, where ϵ indicates the angular extension of the blind zone near the forward-looking direction. According to the literature, the extension of the blind zone and the Doppler bandwidth are inversely proportional: as the Doppler bandwidth increases by exploiting the movement of the vehicle, the extension of the blind zone is reduced. This has a typical value of $\epsilon = 5°$ [25], [26]. Second, the symmetric targets on both sides of the trajectory have the same Doppler history, which leads to ambiguity, that is, in the angular region $[-(\pi/2), -\epsilon] \cup [\epsilon, (\pi/2)]$.

This article focuses on solving the ambiguity problem in the forward-looking direction, but outside the blind zone. Several algorithms have been proposed in forward-looking SAR to tackle this problem. Bistatic SAR [27], [28], for example, uses another transmitter located at a different position from the receiver; in this way, the designed geometry can provide additional information to address the ambiguity problem. Frequency diverse array [29] was designed by performing transmit beamforming after range compensation, and the echo from the desired range region can be extracted from ambiguous echoes, thus providing unambiguous imaging. A multibeam DBS approach was proposed in [30] based on the DBF using a scanning imaging system to provide high cross-range resolution. Multichannel radar in [31] uses the back-projection (BP) algorithm plus MIMO information to solve the ambiguity problem, while at the same time, a curved motion trajectory can be used to improve the poor resolution in the region where look angles are equal or close to zero degrees. However, this algorithm is rather time-consuming, limiting its use in real-time. Different from the above studies, this article proposes an unambiguous Doppler-based forward-looking MIMO radar beam sharpening scan (named short UDFMBSC) method. This combines the DBS with MIMO array processing and jointly provides high angular resolution without ambiguity.

The movement of the car is exploited in this algorithm and characterized in this work. This concept of using the movement of the car to improve angular resolution has been proposed in the literature on the automotive radar. The motion information of the platform to form a synthetic virtual aperture on automotive MIMO radar to obtain high angular resolution is used in [32] and [33]. Two radars approach is proposed in [34]: while one radar is used to determine the vehicle trajectory, another radar utilizes SAR on the known trajectory. The work in [35] uses the residual motion compensation to improve the SAR image quality for automotive. The velocity information was also used for wideband DOA estimation with compensation of range migration and the presence of Doppler ambiguity in [36] and for high angular resolution imaging in [37] and [38].

However, all the aforementioned algorithms [32], [33], [34], [35], [36], [37], [38] do not consider the ambiguity problem in case of the forward-looking radar. To our best knowledge, compared with [21] and [24], this article is the first to solve the ambiguity in DBS for forward-looking MIMO radar. The proposed method does not require any prior information on the environment, the number of targets, and their locations. The method is computationally very efficient, which means it can be implemented easily in current radar sensors.

The main contributions of this article are as follows.

1) An UDFMBSC method is proposed by combining DBS and MIMO array processing to solve the ambiguity problem of symmetric targets in forward-looking automotive radar.
2) The proposed method has been verified for simulated point-like and extended targets, as well as experimental data from a radar sensor, showing that *UDFMBSC* achieves better angular estimation than conventional DBS and digital beam forming (DBF).

The rest of the article is organized as follows. In Section II, the signal model and the fundamentals of DBS are analyzed. The problem formulation and the proposed method are demonstrated in Section III. The simulation results and evaluations of ideal point targets and complex extended targets, as well as the experimental results, are provided in Section IV. Finally, conclusions are drawn in Section V.

II. Signal Model and Fundamentals

A. Signal Model

Frequency-modulated continuous wave (FMCW) MIMO radar with n virtual antennas is considered, here. Without losing generality, the omnidirectional antenna pattern is considered for the transmitter and receiver.

The FMCW chirp is transmitted with chirp duration T_c and pulse repetition interval (PRI) T. A normalized single chirp signal with bandwidth B has the form

$$s_0(t) = \begin{cases} e^{j2\pi(f_0 t + 0.5\mu t^2)}, & t \in [0, T_c] \\ s_{\text{settle}}(t), & t \in [T_c, T] \end{cases} \quad (1)$$

where f_0 denotes the starting frequency of the chirp, $\mu = (B/T_c)$ denotes the frequency modulation rate, and $s_{\text{settle}}(t)$ indicates the signal during the settling time.

The periodic transmitted signal is decomposed into fast-time domain t' and chirp number domain $l = \lfloor (t/T) \rfloor$ as $t' = t - lT, t' \in [0, T_c]$, where $l = 0, 1, 2, \ldots, L_d - 1$, and L_d is the total number of the chirps in one snapshot or frame.

Then the periodically transmitted signal is expressed as

$$s(t) = s(t' + lT) = s(l, t') = s_0(t'). \quad (2)$$

The round-trip delay of the reflected signal from a scatterer for the ith virtual antenna is

$$\begin{aligned} \tau_{\mathbf{o}}(l, t') &= \frac{2\left(D_{\mathbf{o}}(t' + lT) + v(t' + lT)\right)}{c} \\ &\approx \gamma_{\mathbf{o}} + \frac{2v_r(t' + lT)}{c} \end{aligned} \quad (3)$$

where c is the speed of light, $\gamma_{\mathbf{o}} = (2D_{\mathbf{o}}(t' + lT)/c) \ll T_c$, $D_{\mathbf{o}}$ is the distance between antenna and targets $\mathbf{o}$, and v_r is the radial velocity between the radar and the scatterer.

The corresponding received signal can be written as

$$\begin{aligned} r_{(\mathbf{o},i)}(l, t') &= \alpha e^{j\phi_{\mathbf{o},i}} s(t' + lT - \tau_{\mathbf{o}}(l, t')) \\ &= \alpha e^{j\phi_{\mathbf{o},i}} e^{j2\pi\Phi_{\mathbf{o}}(l,t')} \\ &\text{with } t' \in [\gamma_{\mathbf{o}}, T_c] \end{aligned} \quad (4)$$

where α is the constant complex amplitude of the scatterer, and $e^{j\phi_{\mathbf{o},i}}$ is the phase delay of the scatterer $\mathbf{o}$ at the ith virtual element. According to (2), $\Phi_{\mathbf{o}}(l, t')$ has the form

$$\begin{aligned} \Phi_{\mathbf{o}}(l, t') &= f_0(t' - \tau_{\mathbf{o}}(l, t')) + 0.5\mu\left(t' - \tau_{\mathbf{o}}(l, t')^2\right) \\ &\text{with } t' \in [\gamma_{\mathbf{o}}, T_c]. \end{aligned} \quad (5)$$

From the phase of the received signal, the instantaneous frequency of the received signal is extracted as

$$\begin{aligned} f_{\mathbf{o}}(l, t') &= \frac{\partial\Phi_{\mathbf{o}}(l, t')}{\partial t'} \\ &= \left(f_0 + \mu\left(t' - \tau_{\mathbf{o}}(l, t')\right)\right)\left(1 - \frac{\partial\tau_{\mathbf{o}}(l, t')}{\partial t'}\right) \\ &\approx f_0 + \mu t'. \end{aligned} \quad (6)$$

A property of the virtual uniform linear array is that the range difference between scatterers and different receiver antenna pairs will be approximately equal to a constant with respect to the DOA, and the distance between different receiver antennas is d, which is equal to $d = (\lambda/2)$.

Then the phase delay of the different antenna pairs relative to the first transmit and receive pair is obtained by

$$\phi(\mathbf{o}, i) = 2\pi f_0(l, t')\frac{id}{c}\sin\theta. \quad (7)$$

The received signal is then correlated with the conjugate copy of the transmitted signal to get the de-chirped signal of the $\mathbf{o}$th scatterer received by ith element. Considering that automotive radars work in narrow-band conditions, this signal can be written as in the following equation, where for simplicity it is still indicated the complex amplitude of the de-chirped signal:

$$\begin{aligned} z_{(\mathbf{o},i)}(l, t') &= r_{(\mathbf{o},i)}(l, t') \times s^*(l, t') \\ &= \alpha_{\mathbf{o}} \exp\left[j2\pi f_0 \frac{id}{c}\sin\theta\right] \\ &\quad \times \exp\left[-j2\pi\left(f_0\frac{2v}{c}Tl + \mu\gamma_{\mathbf{o}}t'\right)\right] \\ &\quad \times \exp\left[-j2\pi\mu\frac{2v}{c}Tlt'\right]. \end{aligned} \quad (8)$$

When there are k scatterer points in the field of view, the de-chirped signal would be as follows, as the superposition of the contributions of each scatterer:

$$z(i, l, t') = \sum_{\mathbf{o}}^{k} z_{(\mathbf{o},i)}(l, t'). \quad (9)$$

B. DOA Estimation

A number n of range-Doppler matrices (RDMs) is generated, as many as the number of MIMO channels. For the detected scatterer points, the corresponding elements in these matrices are extracted to form a new Doppler angle matrix (DAM) which is used for DOA estimation. The angle profile of the targets could be extracted from the phase delay between different receivers.

After FFT on fast time t' in (9), we obtain the matrix $\mathbf{X}(i, l, r)$. The detected target is located at a certain range bin r_0, the DAM can be modeled as

$$\mathbf{X}(i, l) = \mathbf{X}(i, l, r_0) = \mathbf{s}^{l\times 1} \cdot \mathbf{a}(\theta) + \mathbf{N} \in \mathbb{C}^{l\times i} \quad (10)$$

where $\mathbf{s}$ is the point scatterer reflection coefficient, $\mathbf{a}(\theta)$ is the spatial steering vector, $\mathbf{N}$ is the noise component, and θ is the incident angle of the point scatterer.

1) MIMO Array: For our n virtual elements MIMO array, the steering vector is given by

$$\mathbf{a_a}(\theta) = \left[1, e^{-j2\pi d\sin\theta/\lambda}, \ldots, e^{-j2\pi(i-1)d\sin\theta/\lambda}\right]^T. \quad (11)$$

The DBF algorithm can handle the DOA estimation, and the weight vector $\mathbf{w}_{\text{DBF}}$ that maximizes the output signal power of the array antenna is given by [39]

$$\mathbf{w}_{\text{DBF}} = \frac{\mathbf{a_a}(\theta)}{\sqrt{\mathbf{a_a}^H(\theta)\,\mathbf{a_a}(\theta)}}. \quad (12)$$

The power of the weighted output is

$$\begin{aligned} P_{\text{DBF}}(\theta) &= E\left[\left|\mathbf{w}_{\text{DBF}}^H\mathbf{X}\right|^2\right] \\ &= \frac{\mathbf{a_a}^H(\theta)\,R_{\mathbf{XX}}\mathbf{a_A}(\theta)}{\mathbf{a_a}^H(\theta)\,\mathbf{a_a}(\theta)} \end{aligned} \quad (13)$$

where $R_{\mathbf{XX}} = E[\mathbf{X}^H\mathbf{X}]$ is the autocorrelation matrix of $\mathbf{X}$, and the $[\cdot]^H$ stands for the operation of conjugate transpose.

2) Doppler Beam Sharpening: Assuming that all the targets are static in the radar field of view, the maximum Doppler will be no larger than the one corresponding to the speed of the car itself v_0. So for DBS, we introduce the steering of the Doppler vector

$$\mathbf{a_d}(\boldsymbol{\theta}) = \left[1, e^{-j2\pi 2v_0 T\cos\theta/\lambda}, \ldots, e^{-j2\pi(l-1)2v_0 T\cos\theta/\lambda}\right]^T. \quad (14)$$

The DBS algorithm can also provide the DOA estimation, and the weight vector $\mathbf{w}_{\mathrm{DBS}}$ has the same form as (12).

The power of the weighted output of DBS is

$$\begin{aligned} P_{\mathrm{DBS}}(\theta) &= E\left[\left|\mathbf{w}_{\mathrm{DBS}}^H \mathbf{X^H}\right|^2\right] \\ &= \frac{\mathbf{a_d}^H(\theta) R_{\mathbf{X^H X^H}} \mathbf{a_d}(\theta)}{\mathbf{a_d}^H(\theta)\mathbf{a_d}(\theta)} \end{aligned} \quad (15)$$

where $R_{\mathbf{X^H X^H}} = E[\mathbf{X}\mathbf{X}^H]$ is the autocorrelation matrix of $\mathbf{X^H}$.

C. Derivation of Angular Resolution

1) MIMO Array: To satisfy no ambiguity within the field of view $[-90°, 90°]$, the spatial difference between adjacent sampling points (i.e., MIMO antennas) should be $\lambda/2$.

Under such circumstances, let us assume that there are two targets located at $\theta + \Delta\theta$ and θ. To resolve the two targets, the angle resolution $\Delta\theta$ should satisfy

$$\begin{aligned} &\frac{2\pi d}{\lambda}(\sin(\theta+\Delta\theta) - \sin(\theta)) > \frac{2\pi}{N_a} \\ &\Rightarrow \Delta\theta_a > \frac{\lambda}{Nd\cos(\theta)} \end{aligned} \quad (16)$$

where N_a is the number of spatial sampling points.

2) Doppler Beam Sharpening: For a forward-looking radar borne on a car moving at speed v_0 in the forward direction, the instantaneous Doppler of a static target located at θ will be

$$f_d = \frac{2v_0 f_0}{c}\cos(\theta). \quad (17)$$

Then in order to resolve two closed targets using DBS, the following equation should be satisfied:

$$\begin{aligned} &\frac{2\pi 2v_0 f_0 T}{c}(\cos(\theta+\Delta\theta) - \cos(\theta)) > \frac{2\pi}{N_d} \\ &\Rightarrow \Delta\theta_d > \frac{\lambda}{2N_d T v_0 \sin(\theta)} \end{aligned} \quad (18)$$

where N_d is the number of chirps used for Doppler estimation, which is limited by the coherent processing time. Also, it is clear that where $\theta \in [-\epsilon, \epsilon]$, the resolution will tend to infinity, causing the blind zone problem.

Compared with the two resolutions (16) and (18), one can easily see that the angular resolution of the MIMO array decreases when the look angle of the region becomes larger, while the Doppler has an inverse behavior. With typical values in current automotive radar, specifically, the chirp duration of 100 us and 256 chirps for Doppler estimation, even if influenced by the impact of the angle θ, most of the time, the Doppler can still provide better resolution capability if the ego-vehicle moves faster than 0.5 m/s. The amplification term from Doppler is defined here

$$n = \frac{\Delta\theta_a}{\Delta\theta_d} = \frac{2N_d T v_0}{N_a d}\tan(\theta). \quad (19)$$

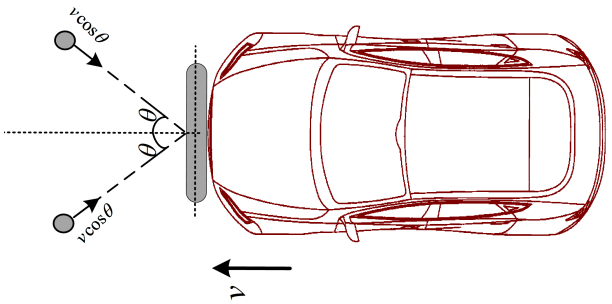

Fig. 1. Schematic of the Doppler ambiguity arising for two symmetric targets in forward-looking radar.

III. Problem Formulation and the Proposed Algorithm

A. Problem Formulation

The Doppler ambiguity comes from the inherent geometry of the forward-looking radar. As shown in Fig. 1, when the car is moving toward the two static targets, both of them will appear symmetric with respect to the boresight of the radar, and they will experience the same Doppler velocity because of the movement of the car. This makes them indistinguishable from using DBS.

Equation (14) shows that the weights of the right- and left-hand positions at the same angle will be the same. Furthermore, the targets will have the same Doppler history, making the conventional DBS-based algorithm ambiguous when used in the forward-looking direction. Hence, it will be hard to decide whether one or two targets are in that direction. Moreover, for the targets shown in Fig. 2(a), the generated response will be the same using the DBS-based method as that of the targets shown in Fig. 2(b). This will cause ghost targets to appear when using the conventional DBS approach.

The DBS approach uses the Doppler information to achieve better angular separation. As the target's movement will introduce an additional Doppler component, the DBS approach suggested cannot focus on the target accurately and the performance of the method will degrade.

B. Modified Steering Doppler Vector Based on Different Vehicle Movements

The DOA estimation algorithm is discussed in II-B. The most important part is the steering vector, from which the time delay patterns of different antennas can be extracted to estimate the targets' angle. For the steering Doppler vector, as the movement of the vehicle will not always be in the forward-looking direction as assumed in II-B, the cross-forward movement also needs to be taken into account. The cross-forward velocity component of the movement will also influence the resulting phase. The error due to this effect

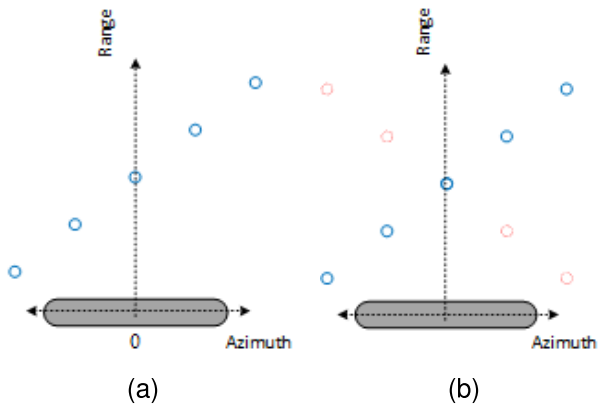

Fig. 2. Schematic of the real scene and the ambiguous view of DBS. (a) Targets in the real scene, while (b) targets when DBS is applied with a red dash marking the ghost targets.

is calculated for each Doppler element as

$$\mathbf{a_c}(\theta) = \left[1, e^{-j2\pi 2\upsilon T \sin\theta/\lambda}, \ldots, e^{-j2\pi(l-1)2\upsilon T \sin\theta/\lambda}\right]^T \quad (20)$$

where υ is the speed of the vehicle in the cross-forward direction. With the compensation factor of the original steering Doppler vector, the new steering vector is given by

$$a_{\mathrm{dc}}(\theta) = a_d(\theta) \odot a_c(\theta) \quad (21)$$

where $\odot$ is Hadamard product.

C. Proposed Method

Generally, one can only detect one target within one range-Doppler resolution cells without any high-resolution finding approach. Hence, the FFT will be applied to the angle vector when extracting the antenna vector from a certain range and Doppler cell to get its spatial frequency. To discriminate between the left-right hand positions in the field of view, the peaks of the auto-convolution of the spatial frequency spectrum were used, here. If only one target is present in the radar of view, even under the Doppler ambiguity condition, the auto-convolution of the spatial frequency spectrum will peak at $f = (2d \sin\theta/\lambda)$. The deduction of this is shown in Appendix I.

If two targets appear in this range-Doppler cell, they must be symmetric to each other, otherwise, they cannot be projected into the same range-Doppler cell. Hence, the auto-convolution of the two targets' spatial frequency spectrum's peak will be in the middle, with the deduction given in Appendix II.

As discussed before, the position of the peak in (34) will provide information on whether there is one target or two. If the peak is in the middle of the function, this means that two targets are present in this Doppler-range index. If the peak is not in the middle, only one target is present. If there is only one target, we can use the DBF results to decide which region the target is located in, that is, the left-hand or the right-hand one. If there are two targets, then there should be two targets symmetric in the radar field of view. One exception to be mentioned is when the target's angle is zero, as in this case, the peak will be in the middle even with only one target.

To summarize, the steps of the proposed approach are described as follows.

Step 1: Estimation of the targets' range.

The range estimation of the targets $\hat{r}$ can be determined by the position of the point corresponding to the targets after FFT.

Step 2: DOA estimation of targets using MIMO array and DBS.

Extract the DAM of the targets' range, then use (13) and (15) to generate the MIMO angle profile $P_{\mathrm{DBF}}(\theta)$ and the DBS angle profile $P_{\mathrm{DBS}}(\theta)$.

Step 3: The proposed UDFMBSC method.

For each searching angle, $\phi \in [-(\pi/2), -\epsilon] \cup [\epsilon, (\pi/2)]$, after finding its corresponding Doppler index named l_ϕ and doing the FFT on the $X(i, l_\phi)$, the spatial frequency spectrum $X(f)$ will be obtained as in (27) in the Appendix. Then the auto-convolution of $X(f)$ is computed to obtain $\chi(\Omega)$.

If the peak of the $\chi(\Omega)$ is in the middle, then there are two targets, and the UDFMBSC angle profile will be

$$P(\phi) = P_{DBF}(\phi) / \max(P_{DBF}(\phi)) \times P_{DBS}(\phi) \ . \quad (22)$$

If the peak of the $\chi(\Omega)$ is not in the middle, there is one target.

The sign of the single target's angle, that is, negative or positive, can be decided by comparing the two values in the MIMO angle profile $P_{\mathrm{DBF}}(\theta)$

$$\mathrm{sign}(\phi) = \begin{cases} 1, & P_{\mathrm{DBF}}(\phi) > P_{\mathrm{DBF}}(-\phi) \\ 0, & P_{\mathrm{DBF}}(\phi) < P_{\mathrm{DBF}}(-\phi). \end{cases} \quad (23)$$

Then the UDFMBSC angle profile will be

$$P(\phi) = \mathrm{sign}(\phi)\, \mathrm{P_{DBF}}(\phi) / \max(\mathrm{P_{DBF}}(\phi)) \times \mathrm{P_{DBS}}(\phi). \quad (24)$$

The algorithm is summarized in the pseudocode shown in Algorithm 1.

IV. Results and Discussion

To show the effectiveness of the proposed method, several results based on simulated ideal point targets and complex extended targets are presented in this section. It is worth mentioning that as the proposed algorithm only focused on the ambiguity problem of forward-looking DBS, that is, in the angular region $[-(\pi/2), -\epsilon]$ $[\epsilon, (\pi/2)]$, the blind zone problem is not considered, here, meaning that the DBS will lose its resolution within $[-\epsilon, \epsilon]$ [25], [26]. It is shown that targets overlapped together in angles when using conventional MIMO array DOA estimation are separated successfully using Doppler sharpening. Also, the ambiguity of the Doppler sharpening is solved effectively by the proposed methods.

A. Ideal Point Targets

A simulated 2×4 MIMO radar was used to demonstrate the proposed UDFMBSC DOA estimation. The underlying assumption of this simulation is that eight channels can be used for DOA estimation in azimuth out of the 12 available in total in commercial 77-GHz automotive radar. The specifications of the radar parameters are listed in Table I.

Algorithm 1 Proposed UDFMBSC Method

Get the range estimation $\hat{r}$

Get the steering vector of MIMO array and compensated steering for Doppler vector $a_a(\theta)$ and $a_{dc}(\theta)$

Perform the DOA estimation on $\hat{r}$ DAM to get the angle profile $P_{DBF}(\theta)$ and $P_{DBS}(\theta)$ as in equations (13) and (15)

for ϕ in $[-\frac{\pi}{2}, -\epsilon] \cup [\epsilon, \frac{\pi}{2}]$do

$l_\phi = (2v\cos\phi N_d T c)/\lambda$

$$X(f) = \sum_{i=-M_\Omega/2}^{M_\Omega/2} X(i, l_\phi)\exp(-j2\pi f i)$$

$$\chi(\Omega) = \sum X(f)X(\Omega - f)$$

if $\chi^{-1}(\max(\chi(\Omega))) = \frac{M_\Omega}{2}$

$P(\phi) = P_{DBF}(\phi)/\max(P_{DBF}(\phi) \times P_{DBS}(\phi)$

else

$P(\phi) = \text{sign}(\phi)\text{P}_{\text{DBF}}(\phi)/\max(\text{P}_{\text{DBF}}(\phi)) \times \text{P}_{\text{DBS}}(\phi)$

where $\text{sign}(\phi)$ is shown in equation (23)

end

endfor

The unambiguous angle profile can be obtained.

TABLE I
CHOSEN RADAR PARAMETERS FOR THE SIMULATION

Parameters	Value
Central Frequency (GHz)	77
Slope (MHz/us)	62.5
Sampling Rate (Msps)	32
Bandwidth (GHz)	1
PRI (us)	100

The MIMO antenna on the forward-looking radar was located at the coordinate center, with targets placed at the same range bin of 10 m to meet the Fraunhofer distance [40] and ensure that targets are in the far-field. The two targets are located at an azimuth angle of 40° and 50° , respectively. When the radar moves with velocity $v_y = 10$ m/s, the proposed approach is compared with the traditional DBF and DBS methods. From Fig. 3, we can see that the proposed approach can well separate the two targets without ambiguity and estimate the position of the two targets at 40.6° and 49.6°, respectively. In contrast, the traditional DBF-based method cannot separate the two targets, and the traditional DBS-based method is ambiguous.

To prove the capability of the proposed method of determining the left and right azimuth quadrants where the targets are located, another simulation is presented in Fig. 4, where the two targets are located at −40° and 50°. It is shown that the proposed approach estimates the position of the two targets as −40.6° and 49.6° proving the effectiveness of the algorithm. Also, to show that the proposed UDFMBSC can determine well, whether there is one target or two, the two targets are symmetrically located at 40° and −40° in another simulation.

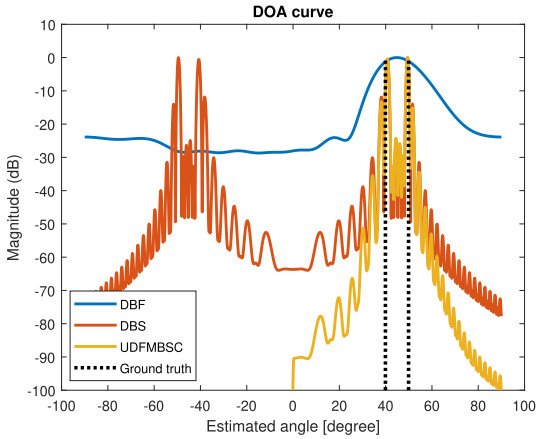

Fig. 3. Simulated performance comparison with the conventional DBF, DBS, and proposed UDFMBSC method. The two point targets are located at 40° and 50° as per ground-truth lines.

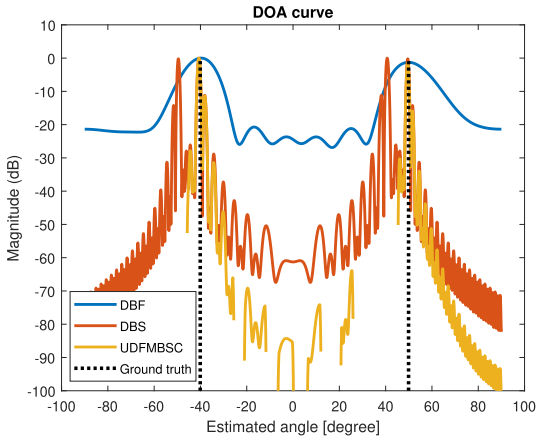

Fig. 4. Simulated performance comparison with the conventional DBF, DBS, and proposed UDFMBSC method. The two point targets are located at −40° and 50° as per ground-truth lines.

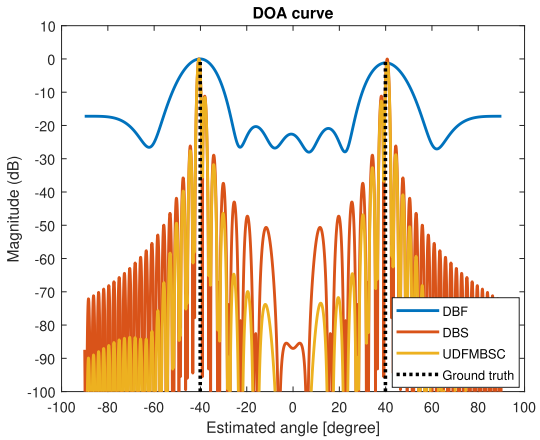

Fig. 5. Simulated performance comparison with the conventional DBF, DBS, and proposed UDFMBSC method. The two point targets are located at −40° and 40° as per ground-truth lines.

The result is shown in Fig. 5 where the proposed method can solve the ambiguity and identify the two actual targets.

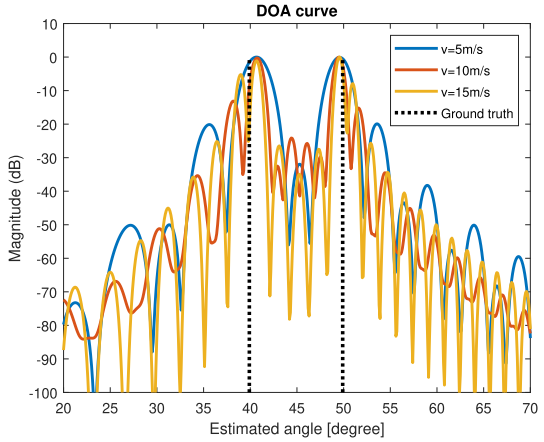

Fig. 6. Simulated performance comparison of the proposed UDFMBSC method under different car speed values. The two point targets are located at 40° and 50° as per ground-truth lines.

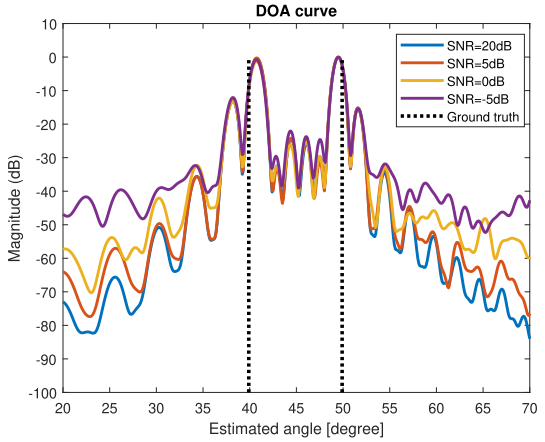

Fig. 8. Simulated performance comparison of the proposed UDFMBSC method for different SNR conditions.

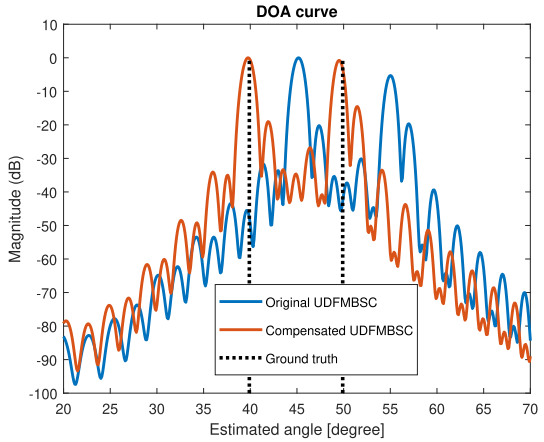

Fig. 7. Simulated performance comparison of the proposed UDFMBSC method with and without compensation. The two point targets are located at 40° and 50° as per ground-truth lines. The car is moving with a cross-forward speed of 1 m/s.

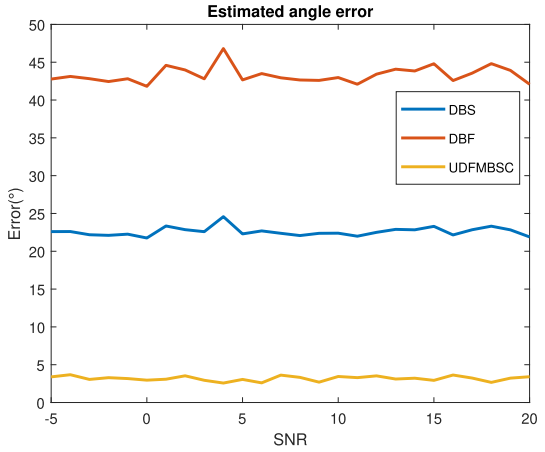

Fig. 9. Monte Carlo test of the estimated error of different algorithms under different SNR.

Also, as shown in Fig. 6, the simulation was tested under different forward speeds. The angle profile of higher speed has a narrower main lobe and lower sidelobe ratio compared with lower speed, showing the resolution and performance of angle estimation will improve by increasing the speed, which is consistence with (19).

In Section III-B, the need for compensation in the steering vector of our proposed method is discussed. The comparison results using simulated point targets located at 40° and 50° and the cross-forward speed of the vehicle equal to 1 m/s with the same simulation settings (i.e., the forward velocity of 10 m/s) are given in Fig. 7. It is shown that the compensation of the velocity in the cross-forward direction, a_c, has a significant impact on the DOA estimation. After compensation, the DOA is accurately estimated as 39° and 49.5°, respectively.

The dependence of the method proposed on the SNR value is shown in Fig. 8. From them, it can be seen that the two targets can be distinguished even under the -5-dB SNR condition, although with raised sidelobes. This suggests that the proposed approach can still work properly for weak targets in challenging SNR conditions. It should be noted that DOA estimation algorithms are generally applied in relatively high SNR conditions; for example, commercial radar units such as those by Bosch or Conti are evaluated on SNR $= 20$ dB [32]. This is reasonable for automotive radar scenarios because it is more important to separate in angle closer targets (hence, with higher SNR values) than targets further away (hence, detected at lower SNR).

To test the robustness of the algorithm, a Monte Carlo test was operated with 1000 repetitions under different SNR conditions. In each test, two point-like targets are placed at random range and angle cells. The results of different DOA algorithms were shown in Fig. 9 in terms of estimation error. To calculate the error, the first two peaks of the angle profile were chosen as the estimated angular positions of the targets, and the error values were calculated by the absolute value of their difference with respect to the ground truth. Because of the ambiguity problem, the conventional DBF-based algorithm yields the worst error, while the traditional DBS-based approach obtains a moderate result. As the Doppler beam is sharper, after solving the ambiguity problem, UDFMBSC gets the best results. All the results show that the estimated DOA

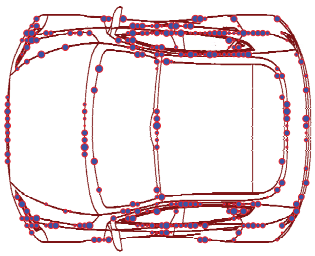

Fig. 10. Extended target model of a car with 273 point scatterers.

values are not much influenced by the different SNR values tested.

Furthermore, the different number of MIMO elements has also been tested, showing only four channels is enough to implement UDFMBSC, which can alleviate the requirement of the MIMO array in azimuth and then could be a potential benefit for 3-D imaging in radar. For example, if fewer antennas are needed for DOA estimation in azimuth, the remaining antennas could be used to improve the estimation in elevation. The minimum for MIMO array processing to determine one target or two in that range-Doppler cell is 4, which means that two transmitters and two receivers will be enough to give a fine angular resolution in azimuth using UDFMBSC.

Finally, what follows is a brief analysis of the computational complexity of the proposed approach, where N_a is the number of virtual antennas for DBF and N_d is the number of chirps used for DBS. Satisfactory performance can be obtained by implementing both the DBF-based method and the DBS-based method in Algorithm 1, hence the computational complexity is related to only an array consisting of $N_a + N_d$ elements in the digital beamforming stage, plus an auto-convolution computation. The computational requirements are only $N_a+N_d+N_d^2$ multiplications and $N_a+N_d^2$ additions. It should be noted that, after the rough estimate of the targets of interest, only a small angular section should be searched to find the peaks. Thus, the computational complexity is about $O(N_a + N_d + N_d^2)$.

B. Complex Extended Targets

To demonstrate the imaging capabilities of the proposed method beyond ideal point targets, simulated models of vehicles perceived as extended targets are used. Each car model is represented by 273 point scatterers generated randomly from the edges of the car as shown in Fig. 10. This model for the extended targets is inspired by the data dome in [41], and the measurements are presented in [42].

Despite being placed around the positions of strong physical scatterers on the vehicle's body, these point scatterers are not meant to mimic precise EM scattering from a car. According to [43], the possible multipath propagation of EM waves due to reflection from the road is not considered in order to simplify the subsequent analysis but without restricting the generality of the proposed imaging approach. The multipath propagation of EM waves due to reflections from the road will influence the received signal, which may result in the appearance of additional points in the image when the specular reflection from the road surface is sufficiently strong (e.g., very smooth road surface, water layer above the road). Furthermore, phenomena of mutual occlusion of scatterers (i.e., one scatter point occluding another located behind it with respect to the radar line of sight) are not modeled for simplicity.

In this work, the amplitude of all scatterers is drawn from the uniform distribution, $\alpha_{\mathbf{o}} = \mathcal{U}(0.5, 1)$. According to the Swerling model III, the amplitude can be seen as a constant during one coherent processing interval. These scatterers are also assumed to be isotropic and provide constant amplitude and phase of the scattered field during the processing period, as in [42]. Using (9), we can simulate the de-chirped signal manually for the cars' scatterers, which are essentially treated as two extended targets. The two cars have the same size with a width of 1.8 m and a length of 4.8 m.

The first simulated scene is with the two static cars located symmetrically with respect to the broadside direction. Both cars are located at a 10-m distance from the radar. The result is shown in Fig. 11. The DBF-based method can only distinguish the two targets without any detailed information, while the DBS-based method provides more details but cannot determine whether the two targets are real or come from ambiguity. The UDFMBSC method can distinguish the two cars and provide more detailed information because of the resulting improvement in angular resolution, making it easier for subsequent processing stages based on these images, such as classification.

The second simulated scene includes again two static cars, this time with spatial separation between them of 3 m as shown in Fig. 12. Also, the cars are located at a 10-m distance from the radar, and the angle is approximately $-30°$. The DBF-based method cannot distinguish two targets because of poor angular resolution, while the DBS-based method can, but it will suffer from the ghost targets in its symmetric region. The proposed UDFMBSC method can not only separate two cars with more detailed information, but also solve the ambiguity problem.

To go beyond the simple visual inspection of images of extended targets, the image contrast metric is introduced in this work to evaluate the separation ability of the proposed method and the other DOA approaches. Image contrast shows the differences in the intensity of each pixel of the image or signal, which are used to evaluate the sidelobe suppression on SAR images [44], [45]. Let us suppose that the two extended targets are better separated because of the improved angular resolution. In that case, the intensity values in the interval between targets will be lower (i.e., there is a gap between them), leading to an increased image contrast value.

The image contrast is defined as

$$C = \frac{\sqrt{E\left\{\left[I^2(i,j) - E\left(I^2(i,j)\right)\right]^2\right\}}}{E\left(I^2(i,j)\right)} \tag{25}$$

where C stands for the image contrast, $I^2(i, j)$ stands for the pixel intensity of (i, j), and $E[\cdot]$ stands for the mean operation.

Also, because of the improved angular resolution, more scatter points within the extended targets can be

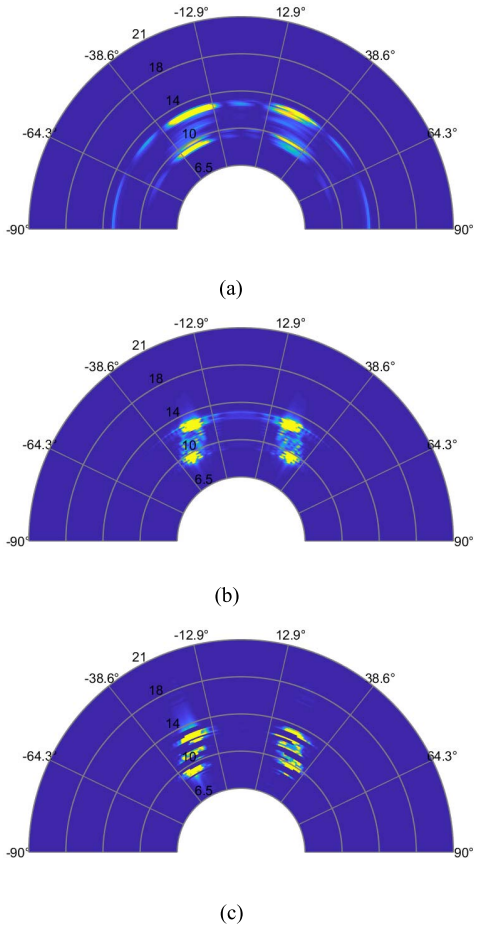

Fig. 11. Resulting images for the two cars symmetrically located with respect to the broadside, when different DOA methods are applied. (a) DBS-based method. (b) DBF-based method. (c) Proposed UDFMBSC method.

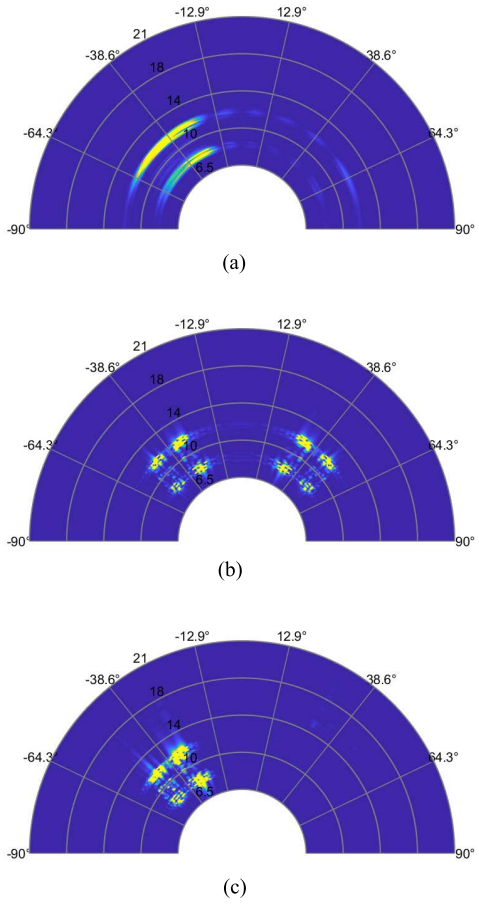

Fig. 12. Resulting images for the two cars located close to each other, when different DOA methods are applied. (a) DBS-based method. (b) DBF-based method. (c) Proposed UDFMBSC method.

detected. Hence, the number of scatterers detected is also used to evaluate the results generated by different algorithms.

A Monte Carlo test is performed where two static cars are placed together in the scene with a spatial separation between them of 3 m. The center position of the two cars is randomly selected in the different repetitions, with the range in the interval [7.5 m, 20 m] and azimuth angle in the interval $[\pm 10°, \pm 45°]$. The resulting image contrasts from the range angle maps generated by different DOA algorithms are shown in Fig. 13. The number of detected scatter points in the scene are also given in Fig. 14. It is shown that UDFMBSC obtains the highest value of the image contrast metric and can detect more scatter points, providing better separation capability as well as better resolution for the considered extended targets. It should be noted that UDFMBSC yields almost the same results as DBS because the evaluations in this test are only calculated with respect to the ground-truth value, so the detrimental problem of ambiguity is not considered here. With UDFMBSC, the image contrast is higher than with DBF, meaning that the proposed methods can get better imaging results.

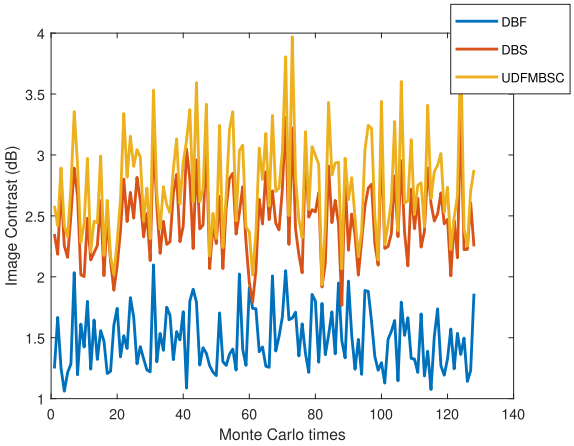

Fig. 13. Image contrast metric as a function of different Monte Carlo tests for different DOA algorithms.

C. Experimental Results

The proposed approach is verified by experimental data. The radar used is the TI IWR6843ISK radar, shown in Fig. 15. The parameters of this radar system are shown in Table. II. Two transmit and four receive antennas are used for azimuth angle estimation during the measurement, and

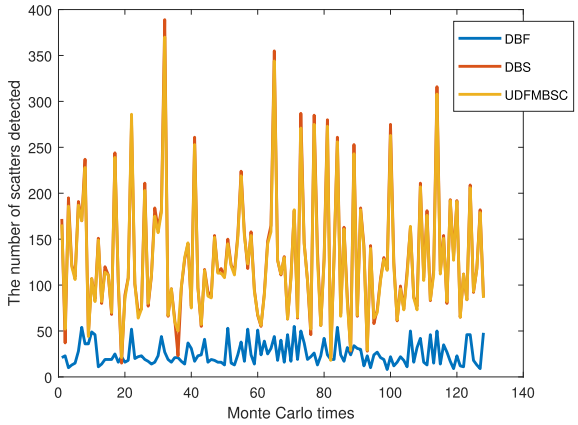

Fig. 14. Number of scatter points detected within the extended targets' region as a function of different Monte Carlo tests for different DOA algorithms.

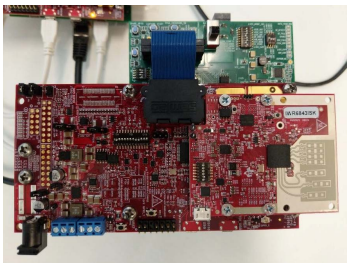

Fig. 15. Radar with the DSP and data capturing boards for experiments.

TABLE II
CHOSEN RADAR PARAMETERS FOR THE EXPERIMENTAL VERIFICATION

Parameters	Value
Central Frequency (GHz)	60
Slope (MHz/us)	10
Sampling Rate (Msps)	2.95
Bandwidth (GHz)	4
Number of chirps in snapshot	128
PRI(us)	420

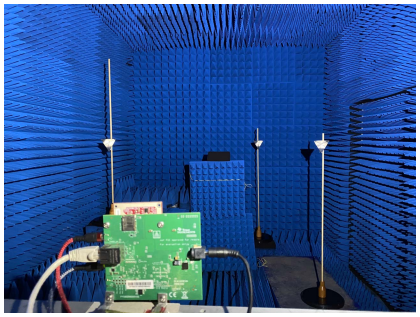

Fig. 16. Experimental scene in the MS3 group's anechoic chamber, with three corner reflectors; two are symmetric with respect to the radar.

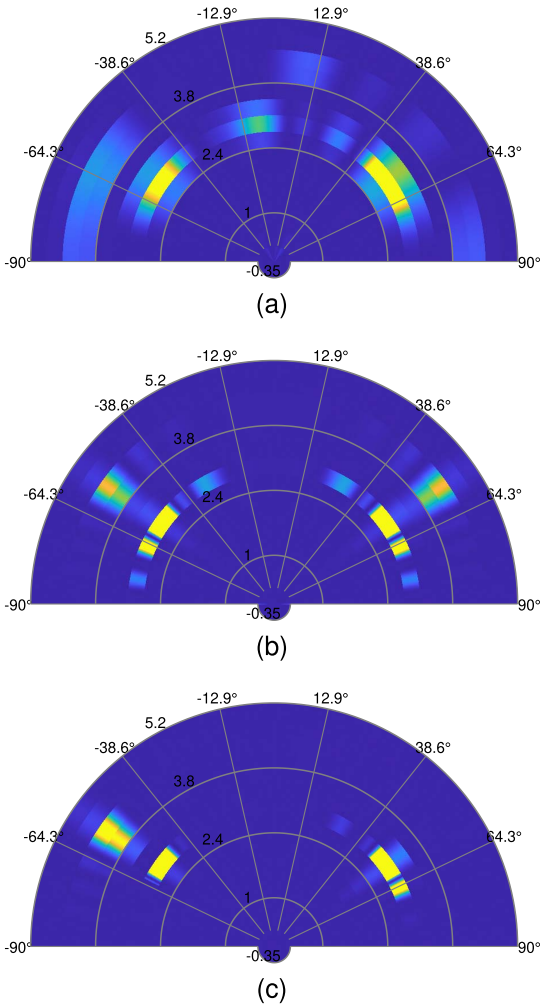

Fig. 17. Experimental results for three corner reflectors. (a) DBS-based method. (b) DBF-based method. (c) Proposed UDFMBSC method.

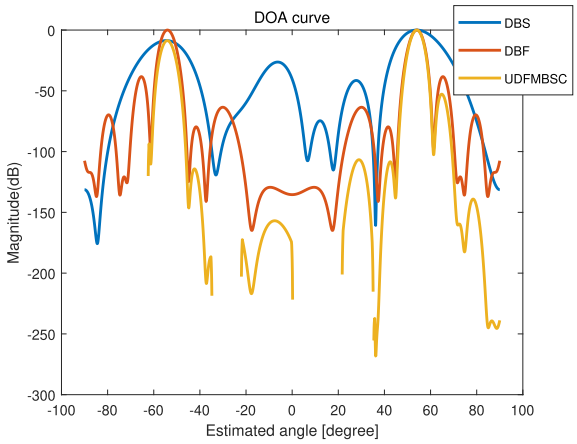

Fig. 18. DOA curve of the two symmetric targets in the experimental test under different methods.

the spacing between adjacent receive antennas is half of the wavelength. The radar is installed on a moving platform, and the experimental measurement campaign was performed in the anechoic chamber at the Delft University of Technology (TU Delft). The experimental scene is shown in Fig. 16.

Because of the limitations of the experimental moving platform, the radar speed is set at $v_y = 0.4$ m/s. The PRI was set as large as possible within the radar limitations to have its best Doppler resolution at the cost of poor range resolution. Because the movement of the radar is limited,

the improvement in the performance of the DBS over DBF is not shown here, but this has been demonstrated in [21], [24], [27], [28], and [29]. The experiment results for the three corner reflectors with different processing methods are shown in Fig. 17. One can see that the two symmetric targets are well imaged, and the third target is unambiguously imaged with the UDFMBSC method, whereas the DBF has a wide mainlobe because of its poor angle resolution, and the DBS is ambiguous in the left/right direction. The angle profile of the two symmetric targets' range bin is also given in Fig. 18.

V. Conclusion

In this article, an UDFMBSC algorithm is proposed, using MIMO array processing in combination with the DBS. Azimuthal resolution improvement, thanks to the DBS, has been demonstrated. Furthermore, for the first time, the Doppler ambiguity has been solved, making it possible to use the DBS to enhance the resolution for forward-looking radar without a high computational cost. Considering the potential cross-forward movement present together with the forward velocity, the modified steering Doppler vector is also defined to compensate for the resulting error.

The proposed method has been verified for simulated point-like and extended targets, as well as experimental data from a radar sensor, showing that UDFMBSC achieves better angular estimation than conventional DBS and DBF. It is worth noting that the proposed approach does not need any prior information on the environment, the number, and the approximate position of targets. The proposed approach is easier to apply in automotive applications in varying scenarios. Furthermore, the method relaxes the requirement of the number of the antenna in the azimuth dimension, making it possible to use a larger array for elevation angle estimation. However, a limitation of the approach is that the target's movement will affect the DBS algorithm and degrade its performance, thus influencing also the performance of the USFMBSC. Also, beyond the ambiguity addressed in this manuscript, the forward-looking DBF method has the limitation of the blind zone problem, which needs to be addressed in future work.

Appendix I
Proof: Auto-Convolution of 1 Target

If there is only one target in a certain range-Doppler cell, the angle vector will be

$$s(l) = \begin{cases} e^{j2\pi \frac{ld\sin\theta}{\lambda}} & l \in [0, N_a] \\ 0 & \text{others.} \end{cases} \tag{26}$$

The spatial frequency spectrum after FFT on this angle vector will be

$$X(f) = \pi N_a \text{sinc}\left(\frac{N_a\left(f + \frac{d\sin\theta}{\lambda}\right)}{2}\right) e^{j\pi N_a\left(f+\frac{d\sin\theta}{\lambda}\right)} \tag{27}$$

where $\text{sinc}(x) = (\sin\pi x/\pi x)$.

According to the convolution theorem, the Fourier transform of the convolution is given by the product of the Fourier transforms of the signal itself.

The Fourier transforms of (27) is as follows:

$$s\left(f'\right) = \begin{cases} 2\pi e^{\left(d\sin\theta f'\right)}, & \left|f' - \frac{\pi N_a}{2}\right| < \frac{\pi N_a}{2} \\ 0, & \text{others.} \end{cases} \tag{28}$$

The convolution of (27) will be the

$$\chi(\Omega) = \int_{-\infty}^{\infty} X(f)\, X(\Omega - f)\, df = \pi^2 N_a \text{sinc}\left(\frac{N_a\left(-\Omega + \frac{2d\sin\theta}{\lambda}\right)}{4}\right) \exp\left[j\frac{\pi N_a}{2}\left(-\Omega + \frac{2d\sin\theta}{\lambda}\right)\right]. \tag{29}$$

So, the peak value will be depended on the target's position term $2d\sin\theta/\lambda$.

Appendix II
Proof: Auto-Convolution of 2 Targets

If there is more than one target in the range-Doppler cell, because of the Doppler symmetric geometry, the targets must be symmetric, so the angle vector will be

$$s(l) = \begin{cases} e^{j2\pi \frac{ld\sin\theta}{\lambda}} + e^{j2\pi \frac{ld\sin(-\theta)}{\lambda}} & l \in [0, N_a] \\ 0 & \text{others.} \end{cases} \tag{30}$$

The Fourier transform of (30) will be

$$\begin{aligned} X(f) = \pi N_a \Bigg(& \text{sinc}\left(\frac{N_a\left(f + \frac{d\sin\theta}{\lambda}\right)}{2}\right) \\ & \times \exp\left[j\pi N_a\left(f + \frac{d\sin\theta}{\lambda}\right)\right] \\ & + \text{sinc}\left(\frac{N_a\left(f + \frac{d\sin(-\theta)}{\lambda}\right)}{2}\right) \\ & \times \exp\left[j\pi N_a\left(f + \frac{d\sin(-\theta)}{\lambda}\right)\right]\Bigg). \end{aligned} \tag{31}$$

Similar to the Appendix before, in order to get the auto-convolution functions, the Fourier transform of (31) is calculated as

$$s\left(f'\right) = \begin{cases} 2\pi\left(e^{\left(d\sin\theta f'\right)} + e^{\left(-d\sin\theta f'\right)}\right), & \left|f' - \frac{\pi N_a}{2}\right| < \frac{\pi N_a}{2} \\ 0, & \text{others.} \end{cases} \tag{32}$$

Then the product of two (32) will be

$$s\left(f'\right) = \begin{cases} 4\pi^2\left(e^{2d\sin\theta f'} + e^{-2d\sin\theta f'} + 2\right), & \left|f' - \frac{\pi N_a}{2}\right| < \frac{\pi N_a}{2} \\ 0, & \text{others.} \end{cases} \tag{33}$$

The auto-convolution function is as follows:

$$\begin{aligned}
&\chi(\Omega)\\
&= \pi^2 N_a \left(\operatorname{sinc}\left(\frac{N_a\left(\Omega + \frac{2d\sin\theta}{\lambda}\right)}{4} \right) \right.\\
&\quad \times \exp\left[j\frac{\pi N_a}{2}\left(\Omega + \frac{2d\sin\theta}{\lambda}\right)\right]\\
&\quad + \operatorname{sinc}\left(\frac{N_a\left(\Omega - \frac{2d\sin\theta}{\lambda}\right)}{4} \right)\\
&\quad \left. \times \exp\left[j\frac{\pi N_a}{2}\left(\Omega - \frac{2d\sin\theta}{\lambda}\right)\right] \right)\\
&\quad + 2\pi^2 N_a \operatorname{sinc}\left(\frac{N_a(\Omega)}{4} \right) \exp\left[j\frac{\pi N_a}{2}(\Omega)\right]. \qquad (34)
\end{aligned}$$

So, the peak will be in the middle of the signal.

ACKNOWLEDGMENT

The authors would like to thank the China Scholarship Council (CSC) for the Ph.D. scholarship for the first author.

REFERENCES

[1] I. Bilik, O. Longman, S. Villeval, and J. Tabrikian, "The rise of radar for autonomous vehicles: Signal processing solutions and future research directions," *IEEE Signal Process. Mag.*, vol. 36, no. 5, pp. 20–31, Sep. 2019.

[2] F. Engels, P. Heidenreich, A. M. Zoubir, F. K. Jondral, and M. Wintermantel, "Advances in automotive radar: A framework on computationally efficient high-resolution frequency estimation," *IEEE Signal Process. Mag.*, vol. 34, no. 2, pp. 36–46, Mar. 2017.

[3] V. Milanés, S. E. Shladover, J. Spring, C. Nowakowski, H. Kawazoe, and M. Nakamura, "Cooperative adaptive cruise control in real traffic situations," *IEEE Trans. Intell. Transp. Syst.*, vol. 15, no. 1, pp. 296–305, Feb. 2014.

[4] M. Ibarra-Arenado, T. Tjahjadi, J. Pérez-Oria, S. Robla-Gómez, and A. Jiménez-Avello, "Shadow-based vehicle detection in urban traffic," *Sensors*, vol. 17, no. 5, p. 975, Apr. 2017.

[5] B. Zhu, J. Zhao, S. Yan, and W. Den, "Personalized lane-change assistance system with driver behavior identification," *IEEE Trans. Veh. Technol.*, vol. 67, no. 11, pp. 10293–10306, Nov. 2018.

[6] J. Hasch, "Driving towards 2020: Automotive radar technology trends," in *IEEE MTT-S Int. Microw. Symp. Dig.*, Apr. 2015, pp. 1–4.

[7] R. Feng, F. Uysal, P. Aubry, and A. Yarovoy, "MIMO–monopulse target localisation for automotive radar," *IET Radar, Sonar Navigat.*, vol. 12, no. 10, pp. 1131–1136, Oct. 2018.

[8] S. M. Patole, M. Torlak, D. Wang, and M. Ali, "Automotive radars: A review of signal processing techniques," *IEEE Signal Process. Mag.*, vol. 34, no. 2, pp. 22–35, Mar. 2017.

[9] F. Roos, J. Bechter, C. Knill, B. Schweizer, and C. Waldschmidt, "Radar sensors for autonomous driving: Modulation schemes and interference mitigation," *IEEE Microw. Mag.*, vol. 20, no. 9, pp. 58–72, Sep. 2019.

[10] J. Wang, P. Aubry, and A. Yarovoy, "3-D short-range imaging with irregular MIMO arrays using NUFFT-based range migration algorithm," *IEEE Trans. Geosci. Remote Sens.*, vol. 58, no. 7, pp. 4730–4742, Jul. 2020.

[11] E. Biglieri, R. Calderbank, A. Constantinides, A. Goldsmith, A. Paulraj, and H. V. Poor, *MIMO Wireless Communications*. Cambridge, U.K.: Cambridge Univ. Press, 2007.

[12] J. Capon, "High-resolution frequency-wavenumber spectrum analysis," *Proc. IEEE*, vol. 57, no. 8, pp. 1408–1418, Aug. 1969.

[13] S. Xu, J. Wang, and A. Yarovoy, "Super resolution DOA for FMCW automotive radar imaging," in *Proc. IEEE Conf. Antenna Meas. Appl. (CAMA)*, Sep. 2018, pp. 1–4.

[14] S. Xu and A. Yarovoy, "Joint Doppler and DOA estimation using 2D MUSIC in presence of phase residual," in *Proc. Eur. Radar Conf. (EURAD)*, Oct. 2017, pp. 203–206.

[15] R. Roy and T. Kailath, "Esprit-estimation of signal parameters via rotational invariance techniques," *IEEE Trans. Acoust., Speech, Signal Process.*, vol. 37, no. 7, pp. 984–995, Jul. 1989.

[16] S. Fortunati, R. Grasso, F. Gini, M. S. Greco, and K. LePage, "Single-snapshot DOA estimation by using compressed sensing," *EURASIP J. Adv. Signal Process.*, vol. 2014, no. 1, pp. 1–17, Dec. 2014.

[17] W. Roberts, P. Stoica, J. Li, T. Yardibi, and F. A. Sadjadi, "Iterative adaptive approaches to MIMO radar imaging," *IEEE J. Sel. Topics Signal Process.*, vol. 4, no. 1, pp. 5–20, Feb. 2010.

[18] T. Yardibi, J. Li, P. Stoica, M. Xue, and A. B. Baggeroer, "Source localization and sensing: A nonparametric iterative adaptive approach based on weighted least squares," *IEEE Trans. Aerosp. Electron. Syst.*, vol. 46, no. 1, pp. 425–443, Feb. 2010.

[19] S. Yuan, F. Fioranelli, and A. Yarovoy, "Improved direction finding accuracy for a limited number of antenna elements with harmonic characteristic analysis," in *Proc. Eur. Radar Conf.*, Milan, Italy, 2022. [Online]. Available: https://ieeexplore-ieee-org.tudelft.idm.oclc.org/document/9924826

[20] J. Chen et al., "Direction finding of linear frequency modulation signal in time modulated array with pulse compression," *IEEE Trans. Antennas Propag.*, vol. 68, no. 1, pp. 509–520, Jan. 2020.

[21] L. Daniel et al., "Application of Doppler beam sharpening for azimuth refinement in prospective low-THz automotive radars," *IET Radar, Sonar Navigat.*, vol. 12, no. 10, pp. 1121–1130, Oct. 2018.

[22] Y. K. Chan and V. C. Koo, "An introduction to synthetic aperture radar (SAR)," *Progr. Electromagn. Res. B*, vol. 2, pp. 27–60, 2008.

[23] C. A. Wiley, "Synthetic aperture radars," *IEEE Trans. Aerosp. Electron. Syst.*, vol. AES-21, no. 3, pp. 440–443, May 1985.

[24] D. Mao, Y. Zhang, Y. Zhang, Y. Huang, and J. Yang, "Super-resolution Doppler beam sharpening method using fast iterative adaptive approach-based spectral estimation," *J. Appl. Remote Sens.*, vol. 12, no. 1, Mar. 2018, Art. no. 015020.

[25] G. W. Stimson, *Introduction to Airborne Radar*. Rijeka, Croatia: SciTech, 1998.

[26] D. Mao, Y. Zhang, Y. Zhang, Y. Huang, and J. Yang, "Doppler beam sharpening using estimated Doppler centroid based on edge detection and fitting," *IEEE Access*, vol. 7, pp. 123604–123615, 2019.

[27] S. Chen, Y. Yuan, S. Zhang, H. Zhao, and Y. Chen, "A new imaging algorithm for forward-looking missile-borne bistatic SAR," *IEEE J. Sel. Topics Appl. Earth Observ. Remote Sens.*, vol. 9, no. 4, pp. 1543–1552, Apr. 2016.

[28] M. Bao, P. Zhou, and L. Shi, "Study on deambiguity algorithm for double antenna forward looking missile borne SAR," *J. Electron. Inf. Technol.*, vol. 35, no. 12, pp. 2857–2862, Feb. 2014.

[29] M. Zhang, G. Liao, X. He, and S. Zhu, "Unambiguous forward-looking SAR imaging on HSV-R using frequency diverse array," *Sensors*, vol. 20, no. 4, p. 1169, Feb. 2020.

[30] Y. Zhang, D. Mao, Y. Zhang, Y. Huang, and J. Yang, "Multi-beam Doppler beam sharpening approach for airborne forward-looking radar imaging," in *Proc. IEEE Int. Geosci. Remote Sens. Symp. (IGARSS)*, Jul. 2017, pp. 6142–6145.

[31] J. Lu, L. Zhang, P. Xie, Z. Meng, and Y. Cao, "High-resolution imaging of multi-channel forward-looking synthetic aperture radar under curve trajectory," *IEEE Access*, vol. 7, pp. 51211–51221, 2019.

[32] W. Zhang, P. Wang, N. He, and Z. He, "Super resolution DOA based on relative motion for FMCW automotive radar," *IEEE Trans. Veh. Technol.*, vol. 69, no. 8, pp. 8698–8709, Aug. 2020.

[33] X. Gao, S. Roy, and G. Xing, "MIMO-SAR: A hierarchical high-resolution imaging algorithm for mmWave FMCW radar in autonomous driving," 2021, *arXiv:2101.09293*.

[34] H. Iqbal, A. Löffler, M. N. Mejdoub, D. Zimmermann, and F. Gruson, "Imaging radar for automated driving functions," *Int. J. Microw. Wireless Technol.*, vol. 13, no. 7, pp. 682–690, 2021.

[35] M. Manzoni et al., "Residual motion compensation in automotive MIMO SAR imaging," 2021, *arXiv:2110.14995*.

[36] S. Xu and A. Yarovoy, "Joint features extraction for multiple moving targets using (ultra-)wideband FMCW signals in the presence of Doppler ambiguity," *IEEE Trans. Signal Process.*, vol. 68, pp. 6562–6577, 2020.

[37] S. Xu, B. J. Kooij, and A. Yarovoy, "Joint Doppler and DOA estimation using (ultra-)wideband FMCW signals," *Signal Process.*, vol. 168, Mar. 2020, Art. no. 107259.

[38] S. Yuan, F. Fioranelli, and A. Yarovoy, "An approach for high-angular resolution implementation in moving automotive MIMO radar," in *Proc. 18th Eur. Radar Conf. (EuRAD)*, Apr. 2022, pp. 449–452.

[39] D. H. Johnson and D. E. Dudgeon, *Array Signal Processing: Concepts and Techniques*. Simon & Schuster, 1992.

[40] G. A. Tyler and B. J. Thompson, "Fraunhofer holography applied to particle size analysis a reassessment," *Optica Acta, Int. J. Opt.*, vol. 23, no. 9, pp. 685–700, Sep. 1976.

[41] A. Chambolle, "An algorithm for total variation minimization and applications," *J. Math. Imag. Vis.*, vol. 20, no. 1, pp. 89–97, 2004.

[42] M. Andres, P. Feil, and W. Menzel, "3D-scattering center detection of automotive targets using 77 GHz UWB radar sensors," in *Proc. 6th Eur. Conf. Antennas Propag. (EUCAP)*, Mar. 2012, pp. 3690–3693.
[43] S. Xu and A. Yarovoy, "Motion-based separation and imaging of closely spaced extended targets," *IEEE Sensors J.*, vol. 20, no. 22, pp. 13542–13551, Nov. 2020.
[44] S. Yuan, Z. Yu, C. Li, and S. Wang, "A novel SAR sidelobe suppression method based on CNN," *IEEE Geosci. Remote Sens. Lett.*, vol. 18, no. 1, pp. 132–136, Jan. 2021.
[45] F. Berizzi and G. Corsini, "Autofocusing of inverse synthetic aperture radar images using contrast optimization," *IEEE Trans. Aerosp. Electron. Syst.*, vol. 32, no. 3, pp. 1185–1191, Jul. 1996.

Sen Yuan (Graduate Student Member, IEEE) was born in Shanxi province, China, in 1998. He received the Bachelor of Engineering degree in electronic information engineering from Beihang University, Beijing, China, in 2017, and the master's degree in the specialty of synthetic aperture radar (SAR) signal processing from Beihang University in 2020 with Prof. C. Li and Dr. Z. Yu. He is currently pursuing the Ph.D. degree in microwave sensing signals and systems with the Delft University of Technology, Delft, The Netherlands, a section within the Department of Microelectronics.

He did an Internship with Tsinghua University, Beijing, about navigation with Dr. X. Chen in 2016. During his graduate education, he studied and became familiar with the SAR, including its satellite orbits, system design, and ground processing. In January 2021, he joined TU Delft. He works on millimeter radar signal processing in automotive applications.

Pascal Aubry received the M.Sc. degree in electronics and microwaves from the Pierre et Marie Curie University, Paris, France, in 1993.

In 1997, he joined TU Delft's International Research Centre for Telecommunication and Radar, Delft, The Netherlands. There, he developed automated measurement software for the outdoors, indoors, and ground-penetrating radar antenna test ranges. He is involved in the testing of antennas and radar systems, as well as designing experimental setups to support research in domains, such as landmine detection, concealed weapon detection, UWB radar imaging, and colored waveforms for MIMO radar, for domestic and European projects.

Francesco Fioranelli (Senior Member, IEEE) received the Laurea (B.Eng., cum laude) and Laurea Specialistica (M.Eng., cum laude) degrees in telecommunication engineering from the Università Politecnica delle Marche, Ancona, Italy, in 2007 and 2010, respectively, and the Ph.D. degree from Durham University, Durham, U.K., in 2014.

He was an Assistant Professor with the University of Glasgow, Glasgow, U.K., from 2016 to 2019, and a Research Associate with University College London, London, U.K., from 2014 to 2016. He is currently an Assistant Professor with TU Delft, Delft, The Netherlands. He has authored over 130 publications between book chapters, journal and conference papers and edited the book on *Micro-Doppler Radar and Its Applications* and *Radar Countermeasures for Unmanned Aerial Vehicles* (IET-Scitech in 2020). His research interests include the development of radar systems and automatic classification for human signatures analysis in healthcare and security, drones and UAVs detection and classification, automotive radar, wind farm, and sea clutter.

Dr. Fioranelli received three best paper awards.

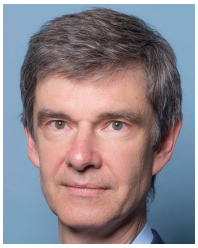

Alexander G. Yarovoy (Fellow, IEEE) received the (Hons.) Diploma degree in radiophysics and electronics and the Phys. & Math. Sci. and Doctor Phys. & Math. Sci. degrees in radiophysics from Kharkov State University, Kharkiv, Ukraine, in 1984, 1987, and 1994, respectively.

In 1987, he joined the Department of Radiophysics, Kharkov State University, as a Researcher and where he became a Full Professor in 1997. From September 1994 to 1996, he was with the Technical University of Ilmenau, Ilmenau, Germany, as a Visiting Researcher. Since 1999, he has been with the Delft University of Technology, Delft, The Netherlands. Since 2009, he has been leading there as Chair of Microwave Sensing, Systems and Signals. He has authored and coauthored more than 450 scientific or technical papers, six patents, and 14 book chapters. His main research interests are in high-resolution radar, microwave imaging, and applied electromagnetics (in particular, UWB antennas).

Prof. Yarovoy is the recipient of the European Microwave Week Radar Award for the paper that best advances the state-of-the-art in radar technology in 2001 (together with L.P. Ligthart and P. van Genderen) and in 2012 (together with T. Savelyev). In 2010, together with D. Caratelli, he got the best paper award of the Applied Computational Electromagnetic Society (ACES). He served as the General TPC Chair of the 2020 European Microwave Week, the Chair and the TPC Chair of the Fifth European Radar Conference, as well as the Secretary of the First European Radar Conference. He served also as the Co-Chair and the TPC Chair of the Tenth International Conference on GPR. He served as an Associated Editor of the *International Journal of Microwave and Wireless Technologies* from 2011 to 2018 and as a Guest Editor of five special issues of the IEEE TRANSACTIONS and other journals. From 2008 to 2017, he served as the Director of the European Microwave Association.